Silicon nanowires to detect electric signals from living cells

Paola Piedimonte[1#], Ivan Mazzetta[2#], Sergio Fucile[3,4], Cristina Limatola[3,4], Elti Cattaruzza[5], Pietro Riello[5], Massimiliano Renzi[3, a)] and Fabrizio Palma[1, b)]

[1]Department SBAI, Sapienza University of Rome, Via Scarpa 14, 00184 Rome, Italy
[2]Department DIET, Sapienza University of Rome, Via Eudossiana 18, 00185 Rome, Italy
[3]Department of Physiology and Pharmacology, Sapienza University of Rome, P.le A. Moro 5, 00184 Rome, Italy
[4]IRCCS Neuromed, Pozzilli, Italy
[5]Department of Molecular Sciences and Nanosystems, Università Ca' Foscari, Dorsoduro 3246, 30123 Venice, Italy

P.P. and I.M. are joint first authors.
a) Corresponding author: massimiliano.renzi@uniroma1.it
b) Corresponding author: fabrizio.palma@uniroma1.it

Abstract. The ability to merge electronic devices with biological systems at the cellular scale is an interesting perspective. Potential applications span from investigating the bio-electric signals in excitable (and non-excitable) cells with an insofar-unreached resolution to plan next-generation therapeutic devices. Semiconductor nanowires (NWs) are well suited for achieving this goal because of their intrinsic size and wide range of possible configurations. However, production of such nanoscale electrodes is pricey, time-consuming and affected by poor compatibility with the Complementary Metal-Oxide-Semiconductor integrated circuits (CMOS-IC) process standards. To take a step forward, we introduced a new method to fabricate small, high-density Silicon NWs (SiNWs) with a fast, relatively inexpensive and low-temperature (200 °C) process. Growth of such SiNWs is compatible with CMOS-IC standards, thus theoretically allowing on-site amplification of bioelectric signals from living cells in tight contact. Here, we report our preliminary data showing the biocompatibility of such SiNWs, as a necessary step to produce a compact device providing super-resolved descriptions of bioelectric waveforms captured from the subcellular to the network level.

1. Introduction

Nanostructured silicon (ns-Si) is considered with increasing interest for its potential in many different applications within modern electronics [1]; this is mainly related to its optical and electrical properties making it unique when compared with bulk silicon [2-11].

Silicon NanoWires (SiNWs) can be considered as a particular form of ns-Si bearing a quite advantageous property: their well-defined separation between each nanostructure, allowing for a large increase of their exposed surface. Together, properties of Si and nanostructures seem very promising to build electronic devices able to detect/condition biological signals at high resolution provided that two major requirements are fulfilled: i) the preparation of SiNWs must be compatible with the CMOS-IC process standards; and ii) SiNWs must be bio-compatible and in tight, structural and functional contact with the living cells.

The growth of NWs is generally obtained by Chemical Vapor Deposition (CVD) on crystalline Si substrates, which requires high-temperature. However, low-temperature is key to make the deposition compatible with other materials, such as plastic, glass, or much more complex substrates as those equipped with integrated circuits (IC). Low-temperature methodology usually requires using metal nanoparticles acting as deposition catalyst, typically gold [12, 13]. Yet, gold is not an IC compatible material due to its very large diffusivity on silicon. An alternative approach is represented by Plasma-Enhanced Chemical Vapor Deposition (PECVD), a powerful method allowing depositing semiconductor thin films from a gas phase precursor at sample temperatures lower than in CVD [14, 15]. PECVD indeed proved successful for NW growth at a relatively fast rate often below the eutectic point of the different catalysts used (e.g., Au [14-16]; Al [17]; Ga or In [16-18]). However, PECVD leads to the formation of mixed amorphous/crystalline structures, making the separation of the deposition by-products from NWs difficult [19]. A crucial point in this field is thus the ability to keep separated the nano-structure and the crystalline form of the deposited material, while working at relatively low-temperature.

We successfully addressed such caveat by growing SiNWs on a Si substrate at relatively low-temperature and heated by microwaves in presence of SiH_4 and Sn droplets working as nano-susceptors (Patent Sapienza N^o: IT0549-17; details are described below and in figure 1), a procedure compatible with the CMOS-IC process standards.

The ultimate aim of our novel approach is producing a new-generation, all-electrical array amenable for high-resolution, large throughput recording of biological signals. Indeed, efficient coupling between cell membrane and recording electrode is a pre-requisite to accurately measure bio-electrical signals from living cells. The techniques mostly used to investigate membrane currents and potentials bear both advantages and limits; thus, the patch-clamp technique, the elective approach for highly-resolved recordings from the neuronal network to single-channel level [20], relies on accessing the interior of single cells, which limits the recording output both in duration and overall number of examined samples. On the other hand, extracellular recording methods, (e.g. Multi-Electrode Arrays, MEA, and multi-transistor arrays [21,22]) are less invasive and allow for long-lasting, multiplexed measurements but only with reduced signal resolution. Assembling an all-electrical device for electrophysiological imaging (that is, a closely packed MEA directly connected to a CMOS capable of high-precision recording from a large network of cells) has long been a major challenge in bioengineering, mostly because of the screening of bio-electrical signals [23,24]. The recent adoption of nanowire transistors and nanotube-coupled transistors connected to CMOS-ICs 25-28] allowed for recordings with significantly improved signal resolution and represented a relevant step forward in the field. Also, CMOS-based MEAs have been very recently combined to laser opto-poration producing long-lasting recordings with good signal-to-noise ratio [29]. However, the latter technologies are still rather pricey and bear little compatibility between CMOS technology and the nanotechnology required to grow small-sized, packed nanowires on site.

Here we describe the production of nano-sized, packed SiNWs using a new methodology bearing two points of strength. First, to acquire electrical signals at high resolution we use an image sensor consisting of a large-scale, high-density and high-sensitivity (6 el/sec) array integrated with CMOS electronics on a single chip. Secondly, to minimize the electrical screening of biological signals we have the Silicon NanoWires (used as nano-detectors) grown directly onto the ICs, thus providing an extremely tight coupling between the cell membrane and the recording device. Of note, our SiNWs on Si-substrates are bio-compatible, as we demonstrated using different cell types.

2. Methods

2.1. Deposition of Silicon NanoWires

SiNWs were grown on a Si substrate (floating zone wafer 1Ω·cm; orientation <100>; 250 μm-thick) by CVD using a vapor-liquid-solid mechanism. The semiconductor wafers were first cleaned with RCA solution (6 parts deionized H_2O, 1-part HCl 27% solution, 1-part H_2O_2

30% solution; 80 °C). At the end of the process, a silicon oxide passivation layer was laid on the silicon surface and in a separate chamber a 5 nm-thick layer of Sn was evaporated onto the silicon oxide layer.

To grow SiNWs, the substrate was baked at 400 °C in a vacuum chamber at 1×10^{-6} mbar pressure under a fast heating regime (3200 °C/h), so to ensure the formation of very small Sn droplets on the substrate surface. The temperature was measured using a thermocouple in contact with the backside of the sample holder (which we will insofar refer to as the 'crucible').

After slow cooling to 200 °C, the sample was exposed for 5 min to plasma in H_2 environment at 600 W under a chamber pressure of 2 mbar and a gas flux of 50 sccm.

In the final step, the sample was processed for 4 min with SiH_4 at 300 W (in absence of plasma activation) with a chamber pressure of 2 mbar and a gas flux of 15 sccm.

2.2. The deposition chamber

The deposition chamber (figure 1) consists of a cylindrical tube allowing for the propagation of only the first TE10 mode of the microwaves field generated by a magnetron at 2.5 GHz and injected into the chamber by an antenna structure. A quartz disc allows for the passage of microwaves while ensuring the preservation of high vacuum in the chamber. The bottom of the chamber consists of a sample holder (the crucible, stainless still or graphite), which serves as substrate induction heater and is fed by a 100 KHz power controller. The position of the crucible can be controlled on the z-axis so to adjust the waveguide conditions. A dielectric spacer is positioned between the surface of the crucible and the sample substrate both to damp the intensity of the tangential electric field of the microwaves and to avoid energy dissipation onto the conducting crucible, rather than onto the Si surface.

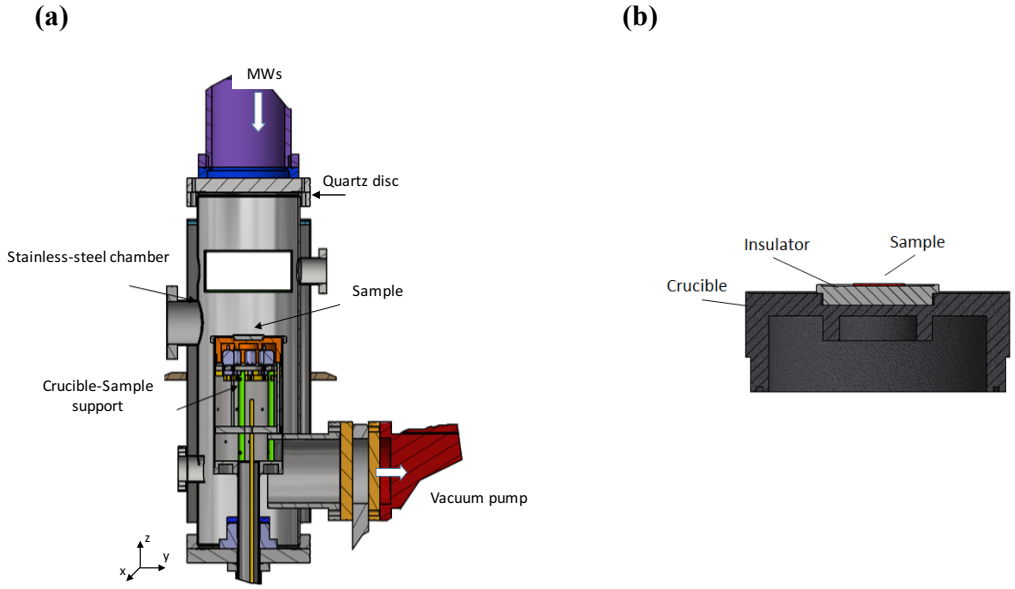

Figure 1. Schematic of the MWCVD deposition chamber (a) and the crucible for substrate heating (b). The sample is located on the crucible sample support bearing a dielectric spacer between the droplet layer and the conductive plane. Because of the tangential electric field concentrated on the sample, Sn droplets are heated up by MWs and work as nano-susceptors.

SiNWs are grown as the result of heating the Si substrate in presence of a thin metal layer: the metal droplets formed do function as nano-susceptors of nanowires which in turn build-up in presence of inflowing silane once the eutectic temperature is overcome. The choice of the metal catalyst is key in our deposition method. Au has long been the metal of choice to grow Si wires and still is the most frequently used catalyst [30-32]. However, recently efforts have been made to find a valid alternative, as using Au induces deep level defects in the Si structure [33], thus making this catalyst scarcely compatible with the CMOS technology

standards. We chose Sn as catalysts material for its full compatibility with our low-temperature fabrication method and so the possibility of on-site growth SiNws on CMOS-ICs [34]. In particular, the phase diagram of the Silicon-Tin system shows a point of eutectic very close to the melting point of pure tin, to the far right of the diagram (5×10^{-5} at.% of Si and 1×10^{-4} °C below the Sn melting point; [35]). Along the deposition process, thanks to the MW irradiation Sn nano-susceptors do overcome the eutectic temperature and trigger the VLS reaction to grow SiNWs even in presence of a limited percentage of SiH_4 and a relatively low substrate temperature (200 °C).

The procedure described leads to the deposition on the silicon substrate of SiNWs with the desired size (typically ~30 nm diameter) and spacing, within some variability (figure 2).

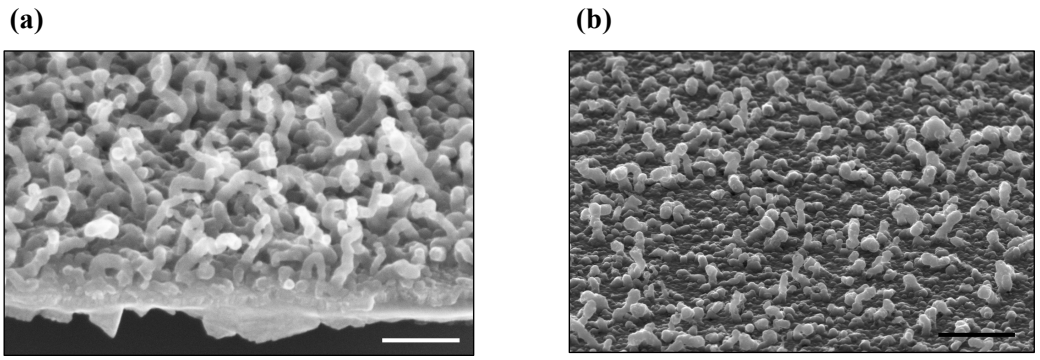

Figure 2. SEM images of typical SiNWs with cross section ~30 nm grown by the MWCVD method on different substrates ((a), silicon; (b), silicon oxide) and used as substrates for cell cultures and physiological recordings. Note the Sn droplets still evident at the nanowire tip. Scale bar: 100 nm.

2.3. Cell Cultures, Patch-Clamp and Ca^{2+} Imaging

2.3.1 Cell Cultures

NG108CC15 cells ('NG cells'; hybrid from mouse neuroblastoma N18TG2 and rat glioma C6BUI cells) were grown in standard conditions (37 ºC; 5% CO_2) using DMEM supplemented with 10% FBS, 100 U/ml penicillin, 0.1 mg/ml streptomycin (P/S), 100 mM Hypoxanthine, 10 mM Aminopterin, and 16 mM Thymidine. NG cells grown in such non-differentiating conditions appeared relatively depolarized and void of mature action potentials, as expected [36]. BV-2 microglial line cells were grown in 10% FBS, 1% P/S DMEM. All cells were plated on uncoated substrates (glass coverslips or SiNWs) and used 24-48 hrs after seeding.

2.3.2 Patch-Clamp and Ca^{2+} Imaging

For patch-clamp, cells were bathed with standard external solution containing (in mM): 145 NaCl, 2 $CaCl_2$, 1 or 2 $MgCl_2$, 4 KCl, 5 HEPES, 5 glucose, 2 Na-pyruvate (pH 7.4, NaOH). The intracellular pipette solution contained (in mM): 110 K-gluconate, 12 KCl, 10 Na_2-Phosphocreatine, 10 HEPES, 0.1 EGTA, 4 Mg-ATP, 0.3 Na-GTP (pH 7.3, KOH; 295 mosm, adjusted with sucrose). The open-tip resistance of borosilicate pipettes ranged from 4.5 to 9.5 MΩ prior to 30~60% compensation. Due to the substrate opacity to transmitted light, cells on engineered substrates were visualized using IR-DIC optics (Leica DM LFS); recordings were acquired using pClamp9 controlling a MultiClamp 700B amplifier (Molecular Devices). In current-clamp experiments, to describe the passive and active properties of NG cells we applied a family of current steps (I_{inj} –200 to +600 pA, 50 pA increments, 1s-long; inter-sweep-interval 1.5 sec; HP –80 mV). Cell input resistance (R_{in}) was calculated as the slope of the linear least-squares fit to the voltage–steady state current relationship corresponding to the first four hyperpolarizing steps. Voltage-sag was estimated as the average percentage decrease of the $|V_m|$ at the steady-state vs peak response to the first three hyperpolarizing

steps [37]. For voltage-clamp experiments, to investigate the expression of voltage-activated Inwardly Rectifying (IR) or Outwardly Rectifying (OR) K^+ channels BV-2 cells were challenged with a family of voltage steps (V_{cmd} –130 to +30 mV, 1-sec long, 20 mV/step, inter-sweep-interval 5 sec; HP –70 mV). The current density was calculated as current/whole-cell capacitance, the latter being estimated using the amplifier compensation circuit.

For Ca^{2+} imaging, cells were loaded with the Ca^{2+}-sensitive fluorescent dye Fura-2 (cell permeant, 2 μM; 45 min at 37 ºC) and recordings were performed in standard external solution (above). Control or agonist (1 mM ATP, 3-sec long application) solutions were delivered by independent tubes positioned 50–100 μm away from the cell and connected to a fast exchanger system (RSC 100, Biologic). Epifluorescence acquisition was driven by Axon Imaging Workbench software (Molecular Devices; 380 nm exc. and 510 nm em. wavelength). All recordings were at room temperature.

3. Results

3.1. Characterization of resulting Silicon NanoWires

The structures we produced are a dense network of individual SiNWs. After SEM characterization, providing information about morphological features of the analyzed samples, a characterization of crystallographic structure and surface chemistry was performed respectively by XRD and XPS analysis. For this analysis the two SEM images of the chosen samples (insofar refer to as sample A and sample B) are reported in figure 3.

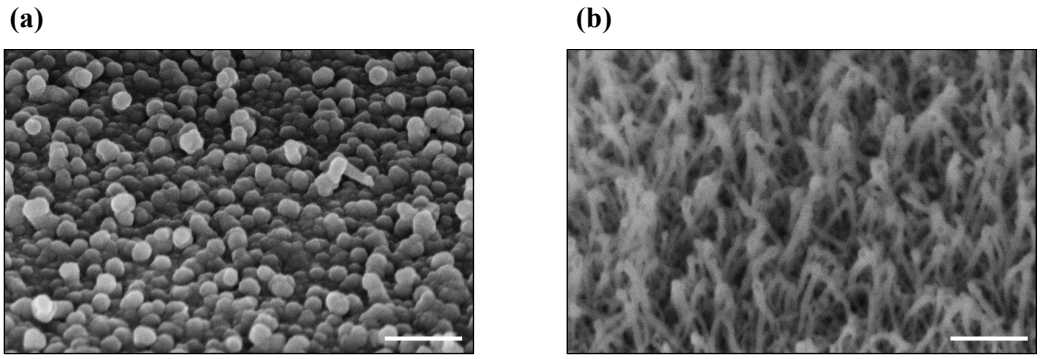

Figure 3. Silicon NWs on sample A (a) and sample B (b). The two samples have been grown with different deposition parameters. Scale bar: 100 nm.

In figure 4(a) the diffraction patterns of the silicon wafer (without NWs) and of the two samples, respectively A and B, are reported.

All the samples, both deposited samples and reference silicon wafer, show the strong (400) peak at 69◦ related to the crystalline substrate. Other very weak peaks appear on the diffraction pattern of the deposited samples and, unexpectedly, different crystal silicon structures, depending on the deposition condition, are observed.

In addition to the usual 400 intense peak of the silicon wafer, the diffraction patterns show one or two very weak peaks that can be ascribed to a metastable BC8-structured silicon phase (Si-III, Spatial group Ia-3, ICSD code 16955 and 246372). The absence of the other peaks proves the highly oriented growth of the nanostructure. Silicon exists in a variety of allotropes at ambient pressure: the most stable cubic diamond silicon (Si-I, Spatial Group Fd-3m) and two metastable BC8-structured Si-III and R8-structured Si-XII that are usually obtained by decompressing the high-pressure phase βSn structured Si-II. BC8-Si, discovered in 1963 by Wentorf and Kasper R.H. [38], has a cubic structure containing one crystallographic unique silicon atom (Wyckoff position 16c). BC8-Si is a direct band gap semiconductor. Among the many different characteristics peculiar of this structure [39], we may cite in particular the low gap (30 meV) as extremely useful for the realization of good contacts.

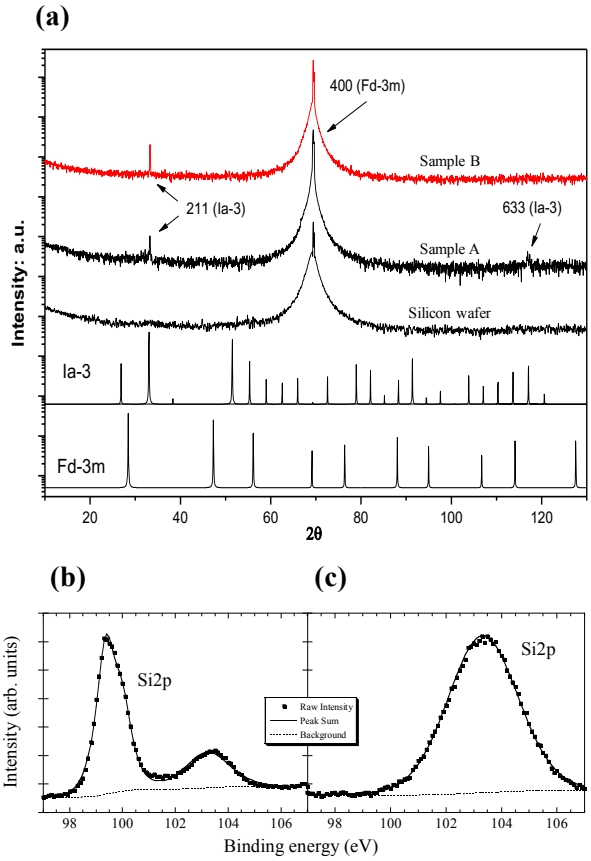

Figure 4. Characterization of crystallographic structure and surface chemistry. In (a), XRD measured diffraction pattern respectively of sample A, B and silicon wafer. At the bottom of the graph, simulated pattern of cubic diamond Si-I respectively with Ia-3 and Fd-3m structure. XPS Si2p band recorded in high-resolution mode, respectively (b) sample A, and (c) sample B.

In XPS analysis, the sample A shows a Si2p signal formed by the overlap of two different components, centered at different BE, as shown in figure 4 (b) and (c). The two components are well resolved, suggesting that the sample is very homogeneous in the analyzed thickness. Being the Si2p spectrum recorded in high-resolution mode, it allowed to fit the two components by using two doublet peaks (Si2p3/2 and Si2p1/2), usually indistinguishable for their limited spin-orbit separation (0.63 eV). The two different constituents of Si2p signal, related to the presence of two different chemical conditions of silicon, are centered at 99.6 eV and 103.4 eV, respectively, suggesting the presence of both metallic Si and dioxide Si, respectively [40]. The Full Width at Half Maximum (FWHM) of the two components is 1.5 eV and 2.5 eV, respectively. The SiKLL signal, not reported, was recorded in order to better identify possible different Si chemical species by means of the silicon "alpha parameter" (binding energy of Si2p band + kinetic energy of SiKLL band: a quantity that is independent by any possible surface charging during X-ray irradiation) [41,42]. The Si alpha parameter allowed to identify again the low-BE component of Si2p as due to metallic silicon (α=1716.6 eV), while the high-BE component (α =1712.8 eV) is confirmed as related to the presence of silicon dioxide [40]. The relative amount of the two chemical species of Si are 70% (Si) and 30% (SiO_2); the presence of SiO_2 is in agreement with both the BE of O1s band (533.0 eV, FWHM=1.8 eV).

The ratio between the amount of oxygen and silicon in this sample is definitely lower than 2, suggesting the presence of sub-stoichiometric silicon oxide too, SiOx ($x<2$): this is in agreement with the large value of the detected FWHM for the Si bands. However, the contemporary enlargement of the O1s, C1s, and N1s bands could be related to an inhomogeneous surface charging of the examined region: this agrees with the possible

presence of Si oxides of different stoichiometry in different point of the analyzed area, and thus with the presence of a slightly different surface charging in different point of the analyzed area. In particular, we point out the possibility that along the nanowire circumference different silicon faces, with different crystallographic orientation, may be exposed, thus offering different opportunity to the bonding with oxygen atoms. Moreover, as explained below, a different local charging could be also related to the particular sample surface shape. Comparing the two samples, sample A surface shows the presence of metallic silicon (about 2/3 of the total amount of Si), completely absent at the surface of sample B. As far the silicon oxide is concerned, in the sample A the Si oxide is stoichiometric and well-defined (SiO_2); in the sample B the presence of silicon oxides of different stoichiometry is highly probable (SiOx, with $x \leq 2$). The different XPS behavior of the two samples is related to their different nanostructure: as shown in figure 4, the surface structure of sample A is characterized by droplets around 50 nm in diameter, while sample B exhibits nanowires of 10 nm in diameter. After the sample synthesis, the air exposure promotes the silicon oxidation of these structures: actually, the thinner nanowires of B are possibly completely oxidized, while the bigger round particles of sample A are reasonably oxidized only in the outer shell, leaving unaffected the metallic silicon core. Moreover, the very rough structure of sample B can also explain an inhomogeneous surface charging, being the tip region of the nanowire very far from the conductive substrate.

3.2. Study of Silicon NanoWires Bio-Compatibility

Once obtained Silicon NWs using an IC-compatible low-temperature process and provided their chemical and crystallographic surface characterization, we stepped onto testing their biocompatibility. Keeping in mind the possible application of our engineered substrates as components for both high-resolution recording devices and conditioning prosthetic implants, we chose to investigate the effects of SiNWs on neuronal and microglial cells.

Thus, we performed patch-clamp experiments on NG108CC15 cells, a hybrid cell line showing some neuronal properties [36]; and BV-2 cells, a murine cell line commonly chosen to model native microglia [43,44]. We also tested SiNWs for biocompatibility using primary cultures from neonatal mice and verified that both hippocampal neurons and microglial cells could be grown on SiNWs with no alteration of their morphology (immunofluorescence preliminary data; not shown). Notably, all cell types tested were successfully grown on engineered substrates. In particular, in current-clamp experiments we found that in response to the injection of hyperpolarizing and depolarizing current steps NG108CC15 cells had both passive properties (resting membrane potential; membrane capacitance; voltage sag and input resistance; not shown) and active response (firing profile) unaltered by the presence of SiNWs as seeding substrate (figure 5, a). Likewise, when investigating BV-2 cells in voltage-clamp experiments to test for their membrane expression of voltage-activated IR or OR K^+ channels [45], we found no difference across seeding conditions (figure 5, b; for patch-clamp experiments, n = 3-to-4 cells per condition; $p>0.3$ or more, unpaired *t*-test when applicable).

To further demonstrate that cells grown on SiNWs do express a pattern of membrane receptors similar to those present in physiological conditions we performed Ca^{2+} imaging experiments on BV-2 cells on SiNWs and found that both basal intracellular [Ca^{2+}] and 1 mM ATP-elicited [Ca^{2+}]$^-$ rise were typical of these cells in normal culture conditions (figure 5, c) [46]. Altogether, our preliminary investigations indicate that SiNWs do not alter normal survival and basic properties of both microglial and neuronal cells *in vitro* thus resulting amenable for non-interfered biological measures.

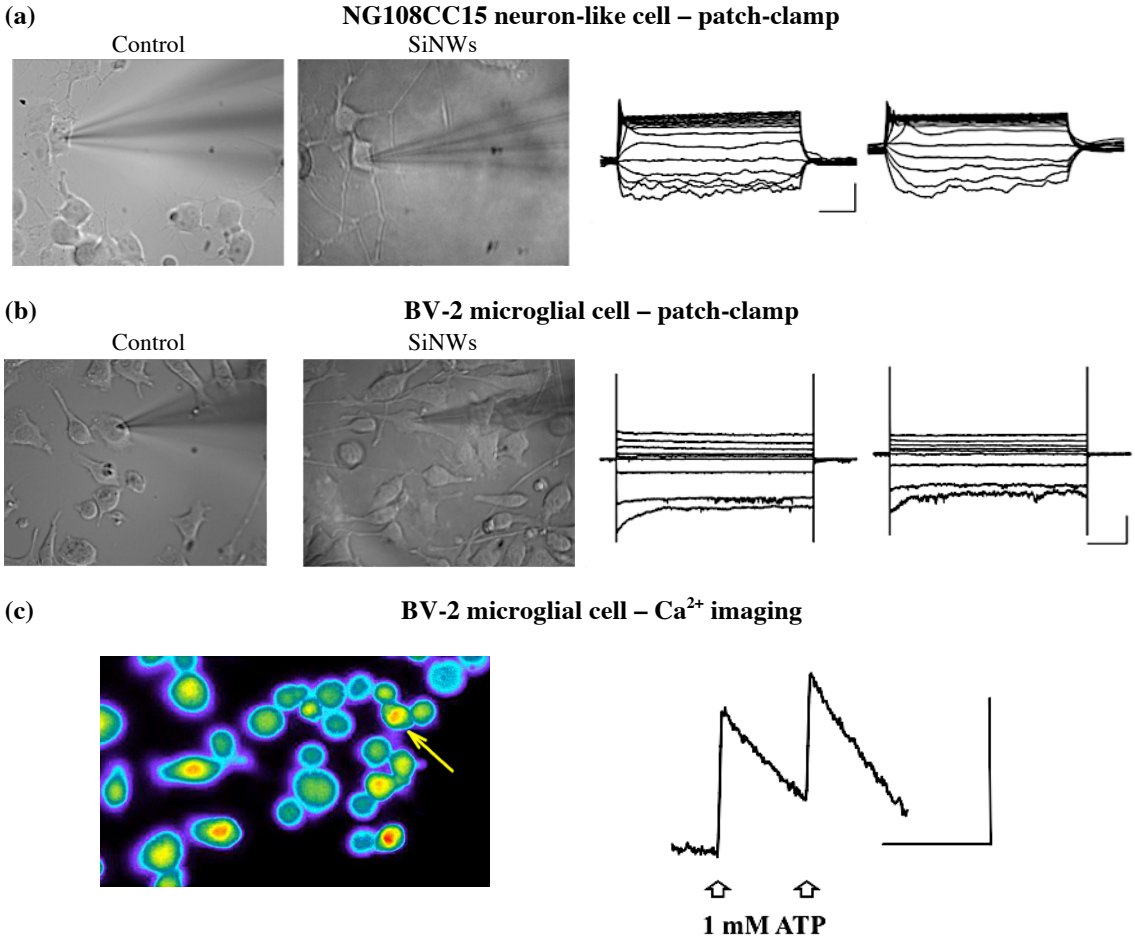

Figure 5. Patch-clamp recording and Ca^{2+} imaging experiments from cells in culture on uncoated glass coverslips (Control) or silicon nanowires (SiNWs), as indicated. (a), current-clamp experiments on NG108CC15 cells. Cells show i) unaltered morphology under IR-DIC visualization (left panels); ii) similar firing profile typical of NG cells kept in non-differentiating culture condition (i.e., lack of spike trains in response to depolarizing injected currents; right panels). (b), voltage-clamp experiments on BV-2 cells. Panels depict lack of difference across seeding substrates for both cell morphology (left) and array of voltage-gated K^+ channels expressed (right). Note that transmitted light images captured in presence of SiNWs appear blurry due to the optical properties of silicon substrates. Scale bars: current-clamp, 100 ms, 20 mV; voltage-clamp, 200 ms, 200 pA. (c), Ca^{2+} imaging experiments from BV-2 cells in culture on SiNWs. Left, typical optic field depicting fura-2 AM loaded cells. The arrow indicates a cell responsive to the fast application of 1 mM ATP. Right, time course of the fluorescence response (indicating $[Ca^{2+}_i]$ rise) to two consecutive applications of ATP (arrows). Typically, we found three-to-four responsive cells per optical field (6 fields analysed across different substrates, no difference found). Bars: fluorescence ratio 0.05; 100 s.

4. Conclusions

In this work we described a novel technology for the fabrication of small, high-density Silicon NanoWires amenable for cell-culturing.

We have shown the possibility to deposit a variety of different nanostructures, at low temperature, using a novel approach in which use of microwaves allows to heat merely the small droplets of metal catalyzer. This new technique is compatible with CMOS technology and could ideally be used to grow nanowires directly on the back-end of ICs. If proved, such approach would let us couple the enormous chemical sensitivity of silicon nanowires and nanostructures with the vast elaboration capability of the electronic integrated circuits.

Using XPS analysis we showed that, beside different conformation, our silicon nanostructures also bear different crystallographic structure, which can be discriminated by

during the deposition process simply adopting different experimental conditions. For instance, with higher energy applied deposited material appears as cubic diamond silicon whilst with lower energy we found evidence of the presence of BC8-Si. This configuration of the crystal (very difficult to obtain otherwise) represents a nanowire feature, which can be particularly useful for the development of integrated sensors due to its very high conductivity.

The chemical analysis of the surface of samples with nanostructured silicon evidenced a high reactivity, with different degree depending on the silicon structures shape.

Notably, we also demonstrated that SiNWs are neutral to living cells and thus potentially amenable to pass electric signals both from and onto cells in tight contact. We are now testing such potential, aiming to produce a compact, all- electrical device for highly resolved cell recording/conditioning.

Acknowledgments

We are deeply grateful to: Aniello Vitulano (Ionvac, Italy) for his dedication with the development of the deposition system; Massimo Izzi and Mario Tucci (ENEA, Italy) for their help with the preparation of substrates; Francesco Mura (Sapienza University of Rome, Italy), for his work collecting SEM images.

References

[1] J. Červenka, M. Ledinský, J. Stuchlík, H. Stuchlíková, S. Bakardjieva, K. Hruška, A. Fejfar, and J. Kočka, Nanotechnology **21**, 415604 (2010).

[2] B. Sun, M. Shao, and S. Lee, Advanced Materials **28**, 10539–10547 (2016).

[3] E. Garnett and P. Yang, Nano letters **10**, 1082–1087 (2010).

[4] A. Blakers and T. Armour, Solar Energy Materials and Solar Cells **93**, 1440–1443 (2009).

[5] J. Yoon, A. J. Baca, S.-I. Park, P. Elvikis, J. B. GEDDES III, L. Li, R. H. Kim, J. Xiao, S. Wang, T.-H. Kim, et al., in Materials for Sustainable Energy: A Collection of Peer-Reviewed Research and Review Articles from Nature Publishing Group (World Scientific, 2011), pp. 38–46.

[6] A. J. Baca, K. J. Yu, J. Xiao, S. Wang, J. Yoon, J. H. Ryu, D. Stevenson, R. G. Nuzzo, A. A. Rockett, Y. Huang, and J. A. Rogers, Energy Environ. Sci. **3**, 208–211 (2010).

[7] M. Sharma, P. R. Pudasaini, F. Ruiz-Zepeda, D. Elam, and A. A. Ayon, ACS applied materials & interfaces **6**, 4356–4363 (2014).

[8] J. Y. Kwon, D. H. Lee, M. Chitambar, S. Maldonado, A. Tuteja, and A. Boukai, Nano letters **12**, 5143–5147 (2012).

[9] S. Guha and J. Yang, Journal of Non-Crystalline Solids **352**, 1917–1921 (2006).

[10] A. I. Boukai, Y. Bunimovich, J. Tahir-Kheli, J.-K. Yu, W. A. Goddard Iii, and J. R. Heath, in Materials For Sustainable Energy: A Collection of Peer-Reviewed Research and Review Articles from Nature Publishing Group (World Scientific, 2011), pp. 116–119.

[11] F. J. DiSalvo, Science **285**, 703–706 (1999).

[12] R. Wagner and W. Ellis, Applied Physics Letters **4**, 89–90 (1964).

[13] V. Schmidt, J. V. Wittemann, S. Senz, and U. Go¨sele, Advanced Materials **21**, 2681–2702 (2009).

[14] J. Červenka, M. Ledinský, J. Stuchlík, H. Stuchlíková, S. Bakardjieva, K. Hruška, A. Fejfar, and J. Kočka, physica status solidi (RRL)–Rapid Research Letters **4**, 37–39 (2010).

[15] S. Hofmann, C. Ducati, R. Neill, S. Piscanec, A. Ferrari, J. Geng, R. Dunin-Borkowski, and J. Robertson, Journal of Applied Physics **94**, 6005–6012 (2003).

[16] H. Griffiths, C. Xu, T. Barrass, M. Cooke, F. Iacopi, P. Vereecken, and S. Esconjauregui, Surface and Coatings Technology **201**, 9215–9220 (2007).

[17] F. Iacopi, P. Vereecken, M. Schaekers, M. Caymax, N. Moelans, B. Blanpain, O.

Richard, C. Detavernier, and H. Griffiths, Nanotechnology **18**, p. 505307 (2007).
[18] L. Yu, B. O'Donnell, P.-J. Alet, S. Conesa-Boj, F. Peiro, J. Arbiol, and P. R. i Cabarrocas, Nanotechnology **20**, p. 225604 (2009).
[19] C. Garozzo, A. La Magna, G. Mannino, V. Privitera, S. Scalese, P. Sberna, F. Simone, and R. Puglisi, Journal of Applied Physics **113**, p. 214313 (2013).
[20] B. Sakmann and E. Neher, Single-channel recording (Springer, 2nd Edn, 1995).
[21] J. Pine, J. Neurosci. Methods 2(1), 19 (1980).
[22] W. Gindl, H. S. Gupta, T. Schöberl, H. C. Lichtenegger and P. Fratz, Applied Physics A 79(8), 2069 (2004).
[23] P. Fromherz, Chem. Phys. Chem. 3(3), 276 (2002).
[24] E.R. Fossum and D.B. Hondongwa, A review of the pinned photodiode for CCD and CMOS image sensors (2014) IEEE J. Electron Devices Soc. 2(3), pp 33–43.
[25] B. P. Timko, T. Cohen-Karni, G. Yu, Q. Qin, B. Tian and C. M. Lieber, Nano Letters, 9(2), 914 (2009).
[26] X. Duan, R. Gao, P. Xie, T. Cohen-Karni, Q. Qing, H. S. Choe, B. Tian, X. Jiang and C. M. Lieber, Nature Nanotechnology 7(3), 174 (2011).
[27] C. Xie, Z. Lin L. Hanson, Y. Cui, and B. Cui, Nature Nanotechnology 7(3), 185 (2012).
[28] J. Abbott, T. Ye, L. Qin, M. Jorgolli, R. S. Gertner, D. Ham and H. Park, Nature nanotechnology 12(5), 460 (2017).
[29] M. Dipalo, H. Amin, L. Lovato, F. Moia, V. Caprettini, G. C. Messina, F. Tantussi, L. Berdondini and F. De Angelis, Nano Letters 17(6), 3932 (2017).
[30] R. S. Wagner and W. C. Ellis, Applied Physics Letters **4**(5), 89 (1964).
[31] W. Chen, P. Pareige, C. Castro, T. Xu, B. Grandidier, D. Stiévenard and P. R. i Cabarrocas, Journal of Applied Physics **118**(10), 104301 (2015).
[32] A. Convertino, V. Mussi and L. Maiolo, Scientific Reports **6**, 25009 (2016).
[33] J. E. Allen, E. R. Hemesath, D. E. Perea, J. L. Lensch-Falk, Z. Y. Li, F. Yin, M. H. Gass, P. Wang, A. L. Bleloch, R. E. Palmer and L. J. Lauhon, Nature Nanotechnology **3**, 168 (2008).
[34] B. V. Schmidt, J. V. Wittemann, S. Senz, and U. Go, Advanced Materials **21**, 2681 (2009).
[35] R. W. Olesinski and G. J. Abbaschian, Bulletin of Alloy Phase Diagrams **5**(3), 273 (1984).
[36] J. Liu, H. Tu, D. Zhang, H. Zheng and Y. L. Li, BMC Neuroscience 13(1), 129 (2012)
[37] B. A. Suter, M. Migliore and G. M. G. Shepherd Cerebral Cortex 23, 1965 (2012).
[38] R. Wentorf and J. Kasper, Science **139**, 338–339 (1963).
[39] H. Zhang, H. Liu, K. Wei, O. O. Kurakevych, Y. Le Godec, Z. Liu, J. Martin, M. Guerrette, G. S. Nolas, and T. A. Strobel, Physical review letters **118**, p. 146601 (2017).
[40] E. Cattaruzza, R. Bertoncello, F. Trivillin, P. Mazzoldi, G. Battaglin, L. Mirenghi, and P. Rotolo, Journal of materials research **11**, 229–235 (1996).
[41] T. Roschek, T. Repmann, J. Mu ̈ller, B. Rech, and H. Wagner, Journal of Vacuum Science & Technology A: Vacuum, Surfaces, and Films **20**, 492–498 (2002).
[42] R. F. Egerton, Reports on Progress in Physics **72**, p. 016502 (2008).
[43] F. Li, J. Lu, C. Y. Wu, C. Kaur, V. Sivakumar, J. Sun, S. Li and E. A. Ling, J. Neurochem. 106(5), 2093 (2008).
[44] S. Rangaraju1, S. A. Raza, A. Pennati, Q. Deng, E. B. Dammer, D. Duong, M. W. Pennington, M. G. Tansey, J. J. Lah, R. Betarbet, N. T. Seyfried and A. I. Levey, Journal of Neuroinflammation 14:128 (2017)
[45] S, Visentin, M. Renzi and G. Levi, GLIA 33, 181 (2001).
[46] L. P. Bernier, A. R. Ase, S. Chevallier, D. Blais, Q. Zhao, E. Boué-Grabot, D. Logothetis and P. Séguéla, J. Neuroscience 28(48), 12938 (2009).